# Zic2 regulates the kinetics of neurulation

**Takeharu Nagai*†, Jun Aruga*‡§, Osamu Minowa¶, Takashi Sugimoto*, Yoshiki Ohno‖, Tetsuo Noda¶, and Katsuhiko Mikoshiba*‡**

*Molecular Neurobiology Laboratory, Tsukuba Life Science Center, RIKEN, Tsukuba, Ibaraki 305-0074, Japan; ‡Developmental Neurobiology Laboratory, Brain Science Institute, RIKEN, Hirosawa, Wako-shi, Saitama 351-0198, Japan; ¶Department of Cell Biology, Cancer Institute, Toshima-ku, Tokyo 170-8455, Japan; ‖Division of Research Facilitation, University of Tsukuba, Tsukuba-shi, Ibaraki 305-8577, Japan; and **Department of Molecular Neurobiology, Institute of Medical Science, University of Tokyo, Minato-ku, Tokyo 108-8639, Japan

Edited by Jeremy Nathans, Johns Hopkins University School of Medicine, Baltimore, MD, and approved December 15, 1999 (received for review August 24, 1999)

**Mutation in human ZIC2, a zinc finger protein homologous to *Drosophila* odd-paired, causes holoprosencephaly (HPE), which is a common, severe malformation of the brain in humans. However, the pathogenesis is largely unknown. Here we show that reduced expression (knockdown) of mouse *Zic2* causes neurulation delay, resulting in HPE and spina bifida. Differentiation of the most dorsal neural plate, which gives rise to both roof plate and neural crest cells, also was delayed as indicated by the expression lag of a roof plate marker, *Wnt3a*. In addition the development of neural crest derivatives such as dorsal root ganglion was impaired. These results suggest that the *Zic2* expression level is crucial for the timing of neurulation. Because the *Zic2* knockdown mouse is the first mutant with HPE and spina bifida to survive to the perinatal period, the mouse will promote analyses of not only the neurulation but also the pathogenesis of human HPE.**

Impairment of the genetic program controlling neural development can cause a wide range of anomalies. Among them, neural tube closure defects (NTD) such as spina bifida and holoprosencephaly (HPE) are the most common congenital malformations in humans. NTD occurs with a combined frequency of 1 in 1,000 live births whereas the frequency of HPE is as high as 1 in every 250 conceptuses (1, 2). These anomalies are etiologically heterogeneous and involve both genetic and environmental factors. However, recent genetic studies in humans and mice are revealing several definite genes involved in these anomalies.

Recently, it was reported that mutations in human *ZIC2* cause HPE (3). ZIC2 is a zinc finger protein homologous to *Drosophila* odd-paired (opa), which is required for the timely activation of a segment polarity gene, *wingless*, in the parasegment of the embryo (4, 5). Mouse *Zic2* is expressed in developing tissues such as neural tissue, somite, and limbs of embryo (6), suggesting the involvement of *Zic2* in mouse development.

To investigate the role of *Zic2* in mouse development, we generated *Zic2* mutant mice, in which the *Zic2* expression is significantly reduced. We found that the reduction of *Zic2* expression resulted in HPE, spina bifida, and some skeletal abnormalities. In the course of neural development, the progression of neurulation was delayed with no changes in the dorsoventral polarity. These results suggest that *Zic2* regulates the progression of neurulation.

## Materials and Methods

**Targeted Mutation of Mouse *Zic2*.** The cloning of the mouse *Zic2* gene, homologous recombination, and generation of chimera mice were performed as described (5, 7). The target vector was designed to replace the first exon that contains the initiator methionine and three of five zinc finger motifs. We obtained several embryonic stem clones, which show the reduction of *Zic2* expression. These clones contained proper recombination at the 3′, but not in the 5′, homologous region. Of these, one clone, which showed a significant reduction of *Zic2* transcript, was used to generate chimeras. We designated the mutated allele $Zic2^{kd}$. The chimera mice first were mated with C57BL/6. The offspring ($Zic2^{kd/+}$) were successively mated twice with C57BL/6 (B6N3). Embryos used in this study were obtained from matings among $Zic2^{kd/+}$ B6N3 mice. The Division of Experimental Animal Research at RIKEN maintained the mice.

**Northern Blot, Reverse Transcription–PCR (RT-PCR), and Immunoblot Analyses.** Northern blot and RT-PCR analysis were performed as described (5, 8), using following primers: *Zic2*, 5′-CAGCTAAGCAATCCCAAGAAAAGCTGCAAC-3′ and 5′-ACAGCCCTCGAACTCACACTGGAAAGG-3′; *Wnt3a*, 5′-TGGGGACTCGGTTCTTACTTGAGGGCG-3′, and 5′-ACCCTAATCTCTCCCCTCCCACCCATC-3′; glyceraldehyde 3-phosphate dehydrogenase, 5′-CCGGTGCTGAGTATGTCGTGGAGTCTAC-3′, and 5′-CTTTCCAGAGGGGCCATCCACAGTCTTC-3′. Comparative expression level of *Zic2* and *Wnt3a* was determined by rectification with the expression level of glyceraldehyde 3-phosphate dehydrogenase. Immunoblot assays were performed with a mAb raised against the peptide His-Arg-Gly-Gly-Ala-Gly-Ser-Gly-Ser-Ser-Gly-Ser-Gly-Gly-Ala-Arg-Arg (amino acids 475–490 in ref. 5), which corresponds to a region unique to the mouse Zic2 protein near the carboxyl terminus.

**Histology, Terminal Deoxynucleotidyltransferase-Mediated UTP End Labeling (TUNEL) Staining, *in Situ* Hybridization.** Sections for general histological analysis were dewaxed in xylene, rehydrated through an ethanol series into PBS, and stained with hematoxylin and eosin. Mitotic cells were detected immunohistochemically by using anti-phospho-histone H3 antibody (Upstate Biotechnology, Lake Placid, NY) and Cy3-conjugated anti-rabbit IgG (Jackson ImmunoResearch). Whole-mount *in situ* hybridization was performed as described (6). Double labeling by *in situ* hybridization was performed as described (9) except that 10% polyvinylalcohol was included in the chromogenic reaction. The TUNEL staining was performed according to the manufacturer's recommendation (*in situ* cell death detection kit, POD, Boehringer Mannheim). Bone and cartilage staining were performed as described (10). Scanning electron micrographs were taken by JEOL JSM-6320F.

## Results

**Generation of *Zic2* Knockdown Mutation.** To clarify the role of *Zic2* in mouse development, we initially attempted to introduce a null

This paper was submitted directly (Track II) to the PNAS office.

Abbreviations: HPE, holoprosencephaly; NTD, neural tube closure defects; RT-PCR, reverse transcription–PCR; TUNEL, terminal deoxynucleotidyltransferase-mediated UTP end labeling; E*n*, embryonic day *n*.

†Present address: Laboratory for Cell Function Dynamics, Brain Science Institute, RIKEN, 2-1 Hirosawa, Wako-shi, Saitama 351-0198, Japan.

§To whom reprint requests should be addressed at: Developmental Neurobiology Laboratory, Brain Science Institute, RIKEN, 2–1 Hirosawa, Wako-shi, Saitama 351-0198, Japan. E-mail: jaruga@brain.riken.go.jp.

The publication costs of this article were defrayed in part by page charge payment. This article must therefore be hereby marked "*advertisement*" in accordance with 18 U.S.C. §1734 solely to indicate this fact.

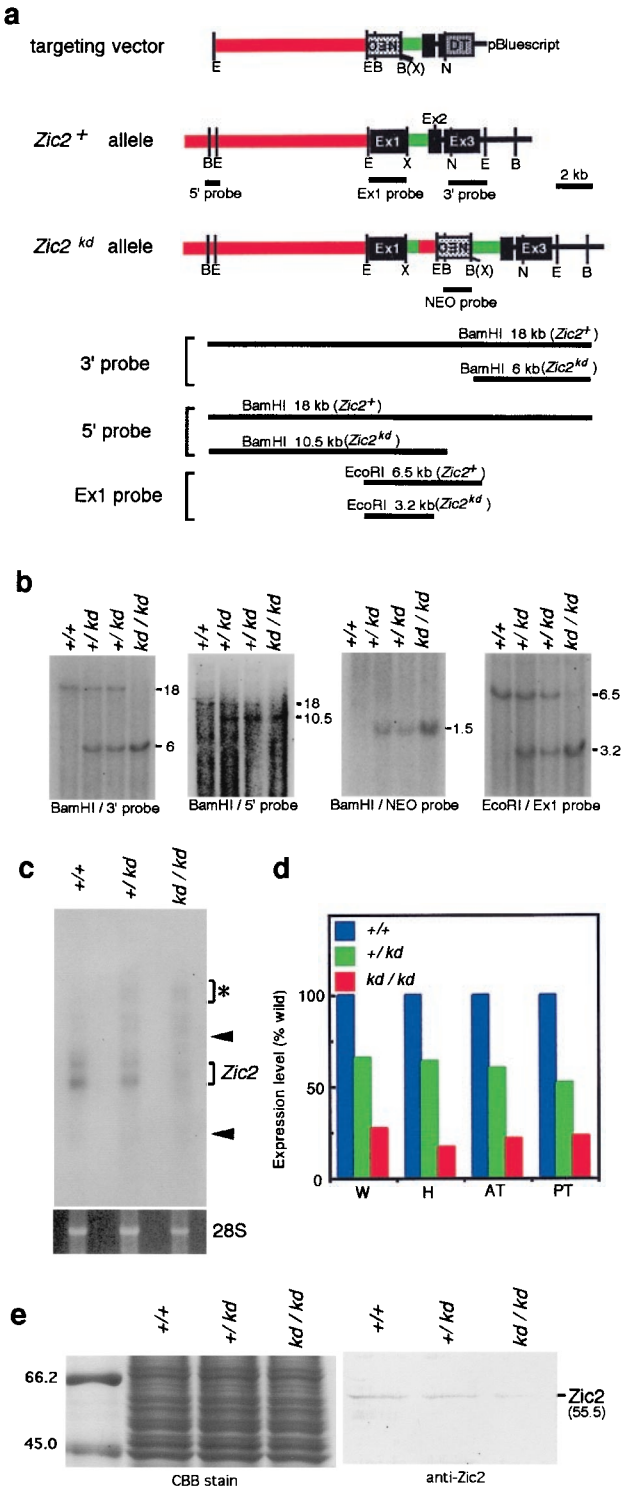


**Fig. 1.** The *Zic2* knockdown mutation. (*a*) Mouse *Zic2* gene, targeting construct, and mutated *Zic2* gene ($Zic2^{kd}$). The targeting vector (*Top*) contains an 8.0-kb and a 2.3-kb region homologous to the *Zic2* gene and a neomycin-resistance gene, respectively, driven by the phosphoglycerate kinase gene (PGK) promoter (NEO). The diphtheria toxin A fragment gene driven by the MC1 promoter (DT) was inserted in the 3′ end of the *Zic2* gene. In the *Zic2kd* allele, a homologous recombination occurred in the 3′ end, whereas a large portion of the 5′ homologous region (red) was deleted and the remaining part was connected to the first intron (green) illegitimately. The connecting point contains the three bases of the overlapping sequence between the 5′ and intron sequence as determined by nucleotide sequencing (data not shown). As a result, PGKneo and 622 bp of the 5′ homologous regions were inserted into the first intron. (*b*) Southern blots verifying the structure of the mutated allele. Genomic DNA was extracted from $Zic2^{+/+}$, $Zic2^{kd/+}$, and $Zic2^{kd/kd}$, digested with *Eco*RI and *Bam*HI, and hybridized with four distinct probes. 5′ and 3′ probes, 5′ and 3′ flanking region of the targeting vector, respectively. Ex1 and NEO probes, fragments containing the *Zic2* exon1 and neomycin-resistance gene, respectively. The expected sizes of restriction fragments are indicated in *a*. (*c* and *d*) The amount of *Zic2* transcript from E11.5 embryonic tissue was measured by Northern blot (*c*) or quantitative RT-PCR analysis (*d*). Expression of the mutated allele was 21% that of the wild-type allele. RNA extracted from E11.5 whole embryo (W), head (H), anterior trunk (AT), and posterior trunk (PT) was analyzed. In *c*, there are additional bands (*) in $Zic2^{kd/+}$ and $Zic2^{kd/kd}$, which correspond to the unspliced mRNA precursor (data not shown), in addition to bands that correspond to the mature transcripts (*Zic2*). Arrowheads indicates the positions of 28S and 18S ribosomal RNA. The bottom frame shows 28S RNA with similar content and integrity. Analysis of RNA from E17.5 embryos gave similar results (data not shown). (*e*) Immunoblot using the anti-Zic2 antibody (*Right*). The density of the bands representing Zic2 protein (55.5 kDa) in the E11.5 $Zic2^{+/+}$, $Zic2^{kd/+}$, and $Zic2^{kd/kd}$ whole embryos was consistent with the amount of *Zic2* transcript shown in *c* and *d*. (*Left*) The total protein used for the immunoblot as revealed by Coomassie blue staining.

mutation into the *Zic2* gene by replacing the first exon with a neomycin-resistance gene. However, the only mutated embryonic stem clones obtained were those in which *Zic2* expression was significantly reduced as a result of unexpected recombination (data not shown). The mutated allele ($Zic2^{kd}$) (Fig. 1*a*) retained the first exon and contained the neomycin-resistance gene at the first intron of *Zic2* as revealed by Southern blot analysis (Fig. 1*b*). Animals heterozygous ($Zic2^{kd/+}$) for this mutation were apparently normal, based on their external appearance and fertility. Genotypes of the embryos were in the ratio expected from Mendelian inheritance [at embryonic day (E) 17–18, $Zic2^{+/+}$, 27%; $Zic2^{kd/+}$, 44%; $Zic2^{kd/kd}$, 29% ($n = 54$)], suggesting that there is little, if any, embryonic lethality of $Zic2^{kd/+}$ and $Zic2^{kd/kd}$. However, $Zic2^{kd/kd}$ animals died soon after birth with multiple anomalies.

Because *Zic2* expression is reduced in $Zic2^{kd/+}$ embryonic stem cells, it is possible that *Zic2* expression is changed in the mice possessing $Zic2^{kd}$ allele. To investigate this, we examined *Zic2* expression at various stages and sites in developing $Zic2^{kd/kd}$ embryos. Northern blot analysis with a probe encompassing all three exons gave two bands (wild-type *Zic2* mRNA) in all genotypes. High molecular weight bands (unspliced mRNA precursors) appeared only in $Zic2^{kd/+}$ and $Zic2^{kd/kd}$ embryos (Fig. 1*c*, data not shown), raising the possibility that aberrant proteins are produced in the embryos. However, it is considered that these precursors are not translated into proteins because mRNA precursors carrying introns are not transported to the cytoplasm (11). The *Zic2* expression was reduced by nearly the same degree, both in individual heterozygous (59% of $Zic2^{+/+}$) and homozygous (21% of $Zic2^{+/+}$) embryos (Fig. 1*c*). Similar results were obtained by RT-PCR analysis of RNA extracted from different regions of the embryos (Fig. 1*d*). In addition, *in situ* hybridization showed that the *Zic2* expression pattern was not altered in $Zic2^{kd/kd}$ embryos and the signal strength was consistent with that of Northern blot and RT-PCR analyses (data not shown). Furthermore, the immunoblot analysis using anti-Zic2 mAb revealed that the amount of Zic2 protein in E11.5 embryos (Fig. 1*e*) corresponded with levels of *Zic2* mRNA (Fig. 1 *c* and *d*). These results indicate that the mutation affects *Zic2* expression levels in general, not at particular developmental stages or in particular tissues. We refer to this type of mutation as a knockdown mutation (12).

**Neural and Skeletal Defects in *Zic2* Knockdown Mice.** In homozygous animals ($Zic2^{kd/kd}$), the most frequent abnormality was spina bifida (51/51 in E9.5-E17.5 $Zic2^{kd/kd}$) (Fig. 2 *a*, *b*, and *v*). The affected lumbosacral region lacked skin (spina bifida with my-

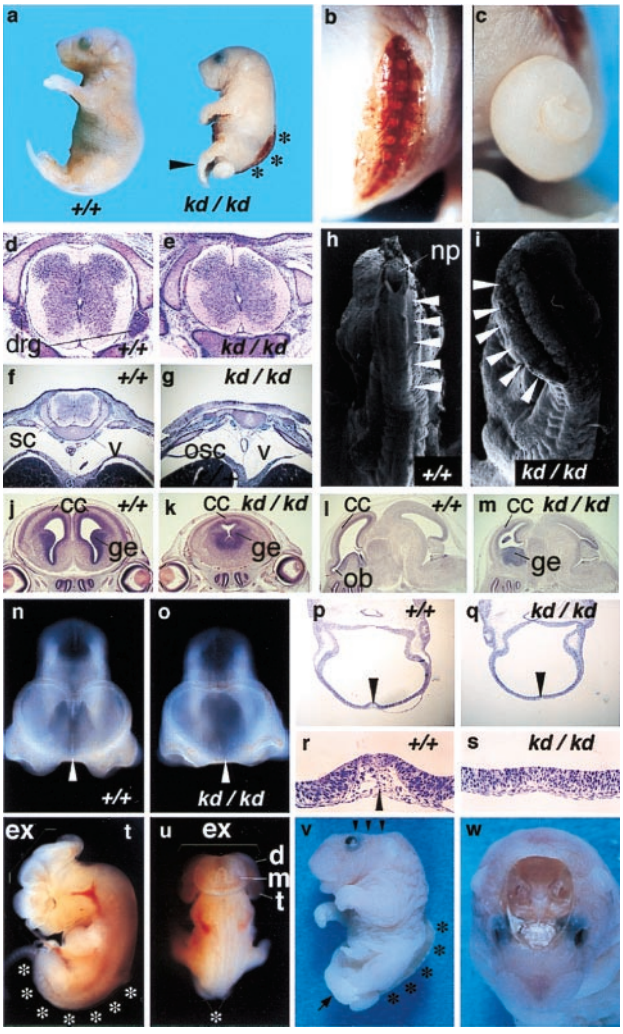


**Fig. 2.** Neural tube defects found in *Zic2*$^{kd/kd}$ mice. (*a*) Lateral views of P0 *Zic2*$^{+/+}$ (*Left*) and *Zic2*$^{kd/kd}$ (*Right*) newborns. Heads of *Zic2*$^{kd/kd}$ animals were significantly smaller (microcephaly). Arrowhead, pes equinus; *, spina bifida. (*b*) Dorsal close-up view of the P0 *Zic2*$^{kd/kd}$ embryo. Spina bifida was always observed. (*c*) Lateral close-up view. Tails were irregularly curled. (*d–g*) Transverse sections through thoracic (*d* and *e*) and lumbar spinal cord (*f* and *g*) of *Zic2*$^{+/+}$ (*d* and *f*) and *Zic2*$^{kd/kd}$ (*e* and *g*) E15.5 embryos. drg, Dorsal root ganglion; sc, spinal cord; osc, open spinal cord; v, vertebral body. (*h* and *i*) Scanning electron micrographs show no closure of lumbar spinal cord in *Zic2*$^{kd/kd}$ embryos (*i*) at E9.5 and successful closure in an E9.5 *Zic2*$^{+/+}$ counterpart (*h*). np, Posterior neuropore. (*j–s*) Holoprosencephaly found in the *Zic2*$^{kd/kd}$ embryo. Coronal (*j* and *k*) and parasagittal (*l* and *m*) sections through cerebrum of *Zic2*$^{+/+}$ (*j* and *l*) and *Zic2*$^{kd/kd}$ (*k* and *m*) E15.5 brain. Cerebral cortex (cc) of both hemispheres in *Zic2*$^{kd/kd}$ brain is fused at the dorsal midline, with the single ventricle and the juxtaposed ganglionic eminence (ge) (*k*). Cerebral cortex and olfactory bulb (ob) of *Zic2*$^{kd/kd}$ brain are hypoplastic (*m*). Magnified frontal views of head (*n* and *o*) and horizontal sections through eye (*p–s*) of *Zic2*$^{+/+}$ (*n*, *p*, and *r*) and *Zic2*$^{kd/kd}$ (*o*, *q*, and *s*) E10.5 embryo. The telencephalic roof plate region in *p* and *q* is magnified in *r* and *s*, respectively. Telencephalic roof plate (arrowheads in *n*, *p*, and *r*) is apparently absent in *Zic2*$^{kd/kd}$ animals (arrowheads in *o* and *q*), resulting in the loss of discrimination between left and right telencephalic vesicles. (*t* and *u*) A typical example of exencephaly found in the E12.5 *Zic2*$^{kd/kd}$ embryo. *p*, Lateral view; *q*, dorsal view. Telencephalic (t), diencephalic (d), and mesencephalic (m) neural plate fail to fuse at the midline [indicated by Ex (exencephaly)]. The spinal cord remains open in the lumbosacral region (*). (*v*) Lateral view of *Zic2*$^{kd/kd}$ embryo (E18.5) possessing anencephaly (arrowheads) and spina bifida (*). (*w*) Top view of embryo in *v*. In this particular animal, almost all brain tissue was lost.

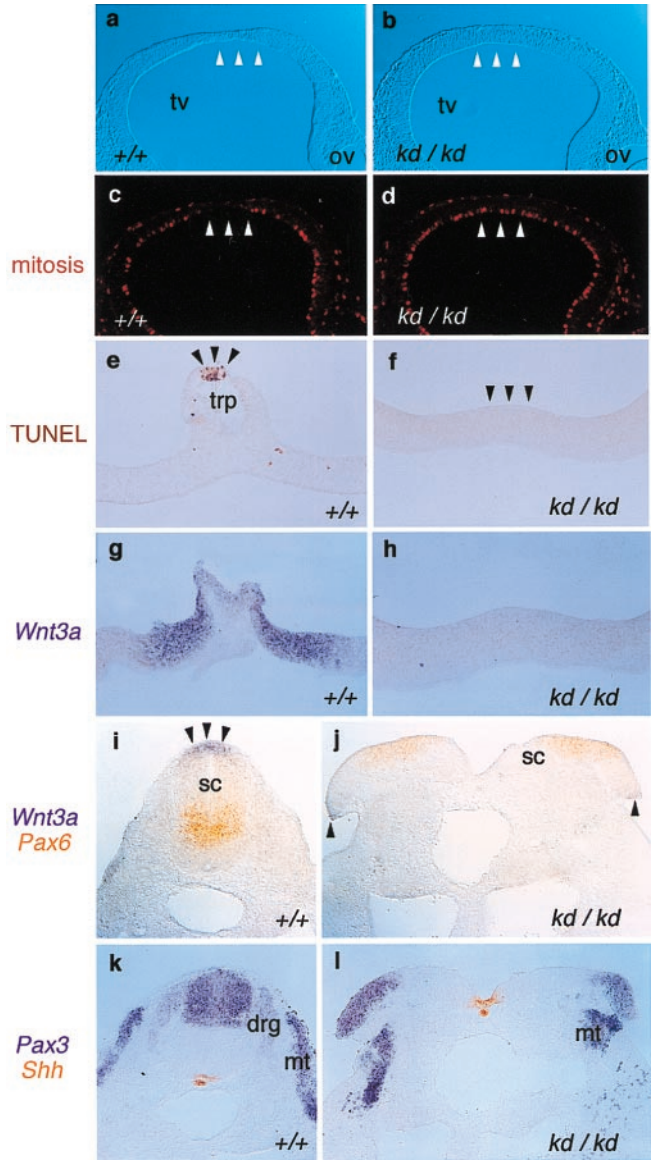


**Fig. 3.** Development of the roof plate is disturbed in the *Zic2*$^{kd/kd}$ embryo. Immunohistochemistry (*a–d*), TUNEL staining (*e* and *f*), and *in situ* hybridization (*g–l*) were performed on *Zic2*$^{+/+}$ (*a*, *c*, *e*, *g*, *i*, and *k*) and *Zic2*$^{kd/kd}$ (*b*, *d*, *f*, *h*, *j*, and *l*). (*a–d*) Immunohistochemical staining using antiphosphohistone H3 antibody to detect mitotic cells in the sections through E9.5 telencephalon. (*a* and *b*) Bright-field view. In the *Zic2*$^{+/+}$ animal, the mitotic cells were scarce in the prospective roof plate region with thinning (arrowheads in *a* and *c*). Such a scarcity or thinning was not observed in the *Zic2*$^{kd/kd}$ animals (arrowheads in *b* and *d*). (*e* and *f*) TUNEL staining of the sections through the E10.5 telencephalic roof plate (trp). In the *Zic2*$^{+/+}$ animal, staining characteristic of dying cells was observed at the midline (*e*, arrowheads) whereas no staining in the corresponding region of *Zic2*$^{kd/kd}$ animals was observed (*f*, arrowheads). (*g–l*) *In situ* hybridization showing the distribution of *Wnt3a* (*g*, *h*, *i*, and *j*, purple), *Pax6* (*i* and *j*, orange), *Pax3* (*k* and *l*, purple), and *Shh* (*k* and *l*, orange), in transverse sections through telencephalic roof plate (*g* and *h*) and through the lumbar spinal cord of E10.5 embryos (*i–l*). Note that *Wnt3a* expression is absent in the telencephalic roof plate (*h*) and reduced in the edges of the open spinal cord (*j*, arrowheads), which corresponds to the roof plate of the properly closed spinal cord (*i*, arrowheads). *Pax3* staining in the dorsal root ganglia (drg) of *Zic2*$^{kd/kd}$ embryos was hardly visible whereas spinal cord (sc) and myotome (mt) staining remained visibly unchanged (*k* and *l*).

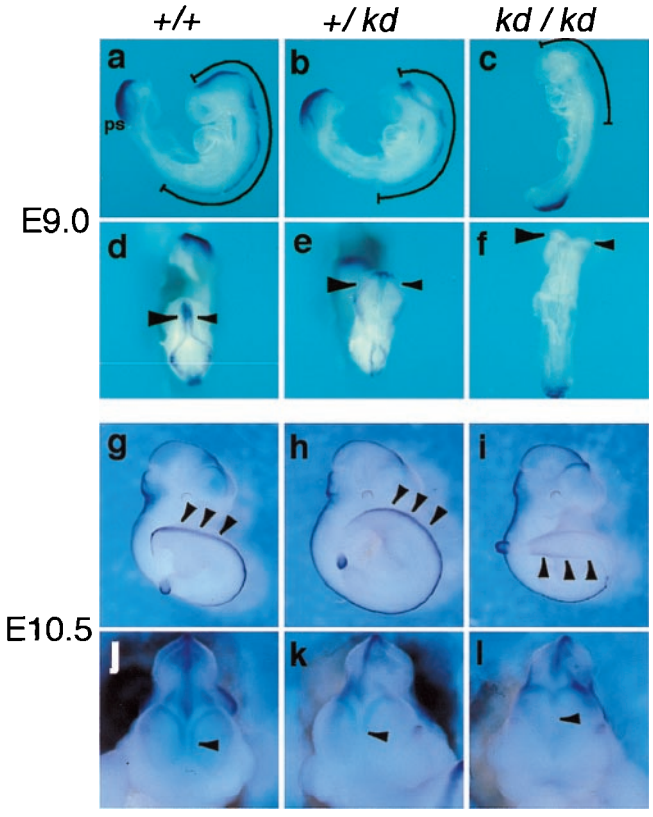


**Fig. 4.** The delay of neurulation is concomitant with the delay of *Wnt3a* expression in *Zic2*$^{kd/kd}$ embryo. Lateral (*a–c* and *g–i*), dorsal (*d–f*), and magnified frontal views (*j–l*) of the E9.0 (*a–f*) and E10.5 (*g–l*) *Zic2*$^{+/+}$ (*a*, *d*, *g*, and *j*), *Zic2*$^{kd/+}$ (*b*, *e*, *h*, and *k*), or *Zic2*$^{kd/kd}$ (*c*, *f*, *i*, and *l*) littermate embryos stained with *Wnt3a* probe by whole-mount *in situ* hybridization. Lines in *a–c* indicate the rostrocaudal extension of the *Wnt3a* expression in the dorsal neural tube. Arrowheads in *d–f* indicate the expression in the dorsal midbrain. The anterior neuropore of *Zic2*$^{kd/kd}$ is not closed (*f*). The arrowheads in *g–i* and *j–l* indicate the lumbosacral expression and telencephalic roof plate expression, respectively. ps; primitive streak region.

eloschisis). Histological examination of E15.5 embryos with spina bifida revealed the eroded area retained remnants of the degenerated spinal cord and the vertebral arches were widely opened (Fig. 2*g*). Concomitant with spinal cord degeneration, the hind limbs of the embryos were paralyzed and crossing each other, and the feet were abnormally pointed and plantar-flexed (pes equinus) (Fig. 2 *a* and *v*). Although the thoracic spinal cord apparently was closed, regions of the dorsal horn were reduced in transverse sections of *Zic2*$^{kd/kd}$ mice when compared with *Zic2*$^{+/+}$ counterparts (Fig. 2 *d* and *e*). It was possible to trace the abnormality back to E9.5 when the posterior neuropore closes. At this stage, abnormal folding of the posterior neural tube was observed (Fig. 2*i*).

The rostral parts of the neural tissue also were affected (Fig. 2 *j–w*). The defects varied from HPE (12/12 in E10.5 *Zic2*$^{kd/kd}$) (Fig. 2 *k*, *o*, and *q*) and microcephaly (18/18 in E17.5 *Zic2*$^{kd/kd}$) (Fig. 2*a*) to exencephaly (Fig. 2 *t* and *u*) and anencephaly (5/43 in E10.5-P0 *Zic2*$^{kd/kd}$) (Fig. 2 *v* and *w*). In most cases of HPE, the cerebral cortex was not completely separated (Fig. 2*k*) and the structures derived from the dorsal forebrain were missing, or rather hypoplastic and contracted (Fig. 2*m*). Corresponding abnormalities were observed in the E10.5 embryo, in which the telencephalic roof plate (lamina terminalis) was missing (Fig. 2 *o*, *q*, and *s*). The mesenchymal cells underlying the region were absent (Fig. 2 *r* and *s*), indicating that neural crest cells derived from dorsal forebrain don't differentiate at this stage. In addition, mitotic cells was not decreased in the dorsal telencephalon of the E9.5 *Zic2*$^{kd/kd}$ embryo (Fig. 3*d*) in contrast to the wild-type embryo in which mitotic cells were scarce in the midline region (Fig. 3*c*). TUNEL staining of transverse sections from E10.5 embryos revealed that apoptosis, which normally occurs in the most dorsal region of telencephalic roof plate of wild-type embryo (Fig. 3*e*), did not occur in *Zic2*$^{kd/kd}$ embryo (Fig. 3*f*). These results suggest that proper differentiation of dorsal forebrain is impaired in the *Zic2*$^{kd/kd}$ embryo.

*In situ* hybridization then was performed to examine the dorsoventral properties of the neural tube. *Pax3* (13) (a dorsal neural tube, dorsal root ganglion, and dermomyotome marker), *Pax6* (13) (a ventral neural tube marker), and *Sonic hedgehog* (*Shh*) (14) (a notochord and floor plate marker) were expressed similarly to wild-type animals at E10.5 (Fig. 3 *i–l*). In contrast, the expression of *Wnt3a* (15) (a roof plate marker) was significantly reduced both in the brain (Fig. 3*h*) and spinal cord (Fig. 3*j*) of *Zic2*$^{kd/kd}$ embryo. The amount of *Wnt3a* transcript in *Zic2*$^{kd/kd}$ embryo was reduced to 22% that of *Zic2*$^{+/+}$ as determined by quantitative RT-PCR analysis (data not shown). These results indicate that the roof plate is mainly defective in the *Zic2*$^{kd/kd}$ neural tube whereas the dorsoventral polarity is essentially normal. In addition, *Pax3* expression in dorsal root ganglion, which is a derivative of neural crest cells originating from the dorsal neural tube, was scarcely seen in the *Zic2*$^{kd/kd}$ embryo (Fig. 3*l*). In accordance with this, dorsal root ganglion was impaired in the thoracic region of E15.5 *Zic2*$^{kd/kd}$ (Fig. 2*e*). Taken together with the fact that *Zic2* is no longer expressed in the migrated neural crest cells such as dorsal root ganglion (6), these results suggest that production of neural crest cells is inhibited in *Zic2*$^{kd/kd}$ embryo because of the dorsal neural tube defect.

How does the dorsal neural tube defect in *Zic2*$^{kd/kd}$ embryo occur? We examined the progression of neurulation by whole-mount *in situ* hybridization using *Wnt3a* probe. At E9.0, *Wnt3a* transcript was detected in both the dorsal primitive streak region and dorsal central nervous system (CNS) (15). In the CNS, the expression extended rostrocaudally from the diencephalon to the fore-limb in the *Zic2*$^{+/+}$ embryo (Fig. 4 *a* and *d*), or to the cervical level in the *Zic2*$^{kd/+}$ (Fig. 4 *b* and *e*). *Wnt3a* expression in *Zic2*$^{kd/kd}$ CNS was first detected faintly (Fig. 4 *c* and *f*) at E9.0, whereas the expression in the primitive streak region was comparable to that in *Zic2*$^{+/+}$ and *Zic2*$^{kd/+}$ (Fig. 4 *a–c*). Concomitant with this delay, the neurulation process also was delayed in the *Zic2*$^{kd/+}$ and *Zic2*$^{kd/kd}$ CNS, and the delay in *Zic2*$^{kd/kd}$ was more severe than that in *Zic2*$^{kd/+}$ (Fig. 4 *b* and *c*). When the development proceeded (E10.5), *Wnt3a* expression was indistinguishable between *Zic2*$^{+/+}$ (Fig. 4*g*) and *Zic2*$^{kd/+}$ (Fig. 4*h*) embryos whereas the expression in unclosed lumbosacral spinal cord of *Zic2*$^{kd/kd}$ remained weak (Fig. 4*i*). A delay in the *Wnt3a* expression also was observed in the forebrain (Fig. 4 *j–l*). The *Wnt3a* expression in *Zic2*$^{kd/kd}$ forebrain started at E11.5, 1 day later than in *Zic2*$^{+/+}$ and *Zic2*$^{kd/+}$ (data not shown). The telencephalic roof plate was formed just after the *Wnt3a* expression with the same delay (data not shown). These results suggest that *Zic2* expression level is closely related to the speed of neurulation. It is possible that timely expression of *Wnt3a* in the dorsal neural plate is required for the progression of normal neurulation because *Wnt-3a* mutant mice frequently show open neural tubes in the lumbosacral region (15).

In addition to neural tissue, skeletal systems were affected in the *Zic2*$^{kd/kd}$ mutant. Abnormalities were found in several bones, particularly vertebrae and limbs (Fig. 5). Vertebral arches were malformed and were not fused at the midline (11/11 in E17.5 *Zic2*$^{kd/kd}$) (Fig. 5 *c* and *d*). In addition, the appearance of vertebral arches along the anterior-to-posterior axis was irregular (Fig. 5 *a* and *b*). Particular malformations were found in the

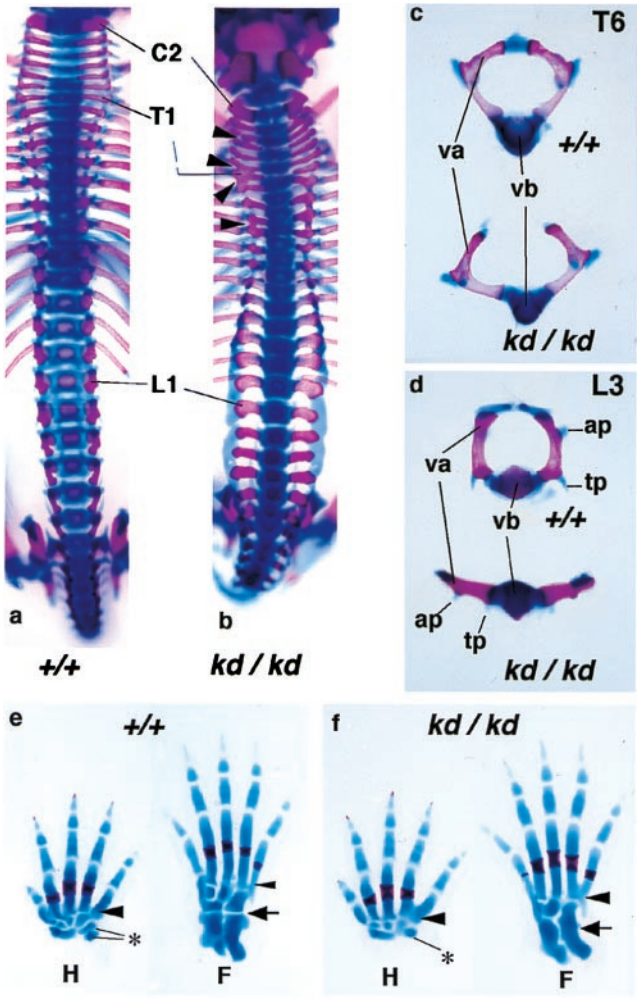


**Fig. 5.** Skeletal abnormalities found in the *Zic2*$^{kd/kd}$ mouse. (*a* and *b*) Dorsal views of the ossified (red) and cartilaginous (blue) axial skeleton from E17.5 *Zic2*$^{+/+}$ (*a*) or *Zic2*$^{kd/kd}$ (*b*) mice. Note that the dorsal aspect of the vertebrae (vertebral arches) was irregularly opened and that abnormal fusions between the rostrocaudally adjacent arches had formed (arrowheads). C2, Cervical vertebra 2; T1, thoracic vertebra 1; L1, lumbar vertebra 1. (*c* and *d*) Comparison of *Zic2*$^{+/+}$ (*Upper*) and *Zic2*$^{kd/kd}$ (*Lower*) thoracic vertebra 6 (*c*, T6) and lumbar vertebra (*d*, L3). ap, Articular process; tp, transverse process; va, vertebral arch; vb, vertebral body. (*e* and *f*) Hand (H) and foot (F) skeletal patterns also were disorganized. The fourth and fifth metacarpal/metatarsal bones were abnormally fused in the *Zic2*$^{kd/kd}$ mouse (*f*) whereas such fusion was not noted in the *Zic2*$^{+/+}$ mouse (*e*) (arrowheads). Similarly, abnormal fusion was found in the carpal (*) and tarsal bones (arrow).

limb skeleton as well. Fourth and fifth metatarsal and metacarpal bones were laterally fused (Fig. 5 *e* and *f*). Abnormal connections also were observed in adjacent carpal and tarsal bones (both were found in 11/11 of the E17.5 *Zic2*$^{kd/kd}$ animals) (Fig. 5 *e* and *f*).

## Discussion

**Comparison to Human *ZIC2* Deficiency.** In the course of this study, the human *ZIC2* gene was found to be responsible for the human HPE (13q32 subgroup) (3). The study reported four cases of ZIC2 haploinsufficiency, with HPE ranging from semilobar to alobar without major facial malformation. The brain phenotypes in the *ZIC2*-deficient patients are similar to those in the *Zic2*$^{kd/kd}$ mutant in which the dorsal midline structures of the prosencephalon were missing or severely malformed. In terms of the type of mutation, *Zic2*$^{kd/kd}$ allele may partially mimic the *ZIC2* haploinsufficiency in humans because the *Zic2* expression is reduced irrespective of tissue or developmental stage. Further analysis of the mouse may lead to a more comprehensive understanding of the pathogenesis and treatment of HPE.

In contrast to HPE, the spina bifida was not reported as a sign of *ZIC2* mutation, perhaps because of the category of the disease. Because spina bifida has been classified as a different class of malformation, it might have been left out of the diagnosis. Otherwise, the appearance of the spina bifida may reflect the amount of Zic2 protein because *Zic2* expression is reduced to 20% in *Zic2* knockdown mice, less than in human *ZIC2* haploinsufficiency. It is possible that a reduction of Zic2 by half causes HPE and more reduction causes both HPE and spina bifida.

The digital anomalies found in the *Zic2*$^{kd/kd}$ mice were not found in HPE patients with the *ZIC2* mutation. In the mouse embryo, *Zic2* is expressed in the distal mesenchyme and the precartilaginous condensations of the limb buds (6). The expression pattern may well correspond to the abnormality. Interestingly, digital abnormality was a consistent feature of the 13q32 deletion syndrome caused by a deletion around locus 13q32 at which *ZIC2* locates (16). The absence of the limb abnormality in the patients with *ZIC2* mutation suggests the existence of other genes, which may act cooperatively with *ZIC2,* located in 13q32, or a functional difference between mouse Zic2 and human ZIC2.

**HPE in the *Zic2*$^{kd/kd}$ Mice.** This study may shed light on the molecular genetic basis of HPE. At present, the disturbance of ventral induction is considered to play a role in the development of HPE (17, 18). Shh, the signal of ventral induction, is responsible for a familial HPE in humans (17). Correspondingly, *Shh*-deficient mice show HPE (18). However, there seems to be significant differences in HPE phenotype between *Zic2* and *Shh* mutants. HPE caused by *Shh* mutation involves facial malformations, such as eye defects ranging from cyclopia to narrowly separated eyes and midline facial clefts (17, 18). In contrast, neither *Zic2*$^{kd/kd}$ mice nor the *ZIC2*-deficient patients show obvious abnormalities in the face (3). In addition, small, but significant, numbers of the *Zic2*$^{kd/kd}$ mice showed exencephaly and anencephaly, which were not found in the *Shh*-deficient mice. These results suggest that another mechanism, different from the disturbance of the ventral induction, is involved in the development of HPE. Alternatively, HPE in *Shh* mutant may be mediated by the change of the *Zic2* expression level in dorsal forebrain because *Zic2* expression in the neural tube is negatively regulated by a factor, possibly Shh, secreted from axial mesoderm (6).

**NTD in the *Zic2*$^{kd/kd}$ Mice**. NTD in the *Zic2*$^{kd/kd}$ mice are characterized by failures of both posterior neural tube closure (spina bifida aperta) and anterior neural tube closure (exencephaly, anencephaly). The anomalies may be caused by the defect intrinsic to the neural plate because *Zic2* is expressed in the dorsal neural plate (6). In this paper, we showed the impaired differentiation of dorsal neural plate (neurulation delay) in *Zic2*$^{kd/kd}$ embryo, which is concomitant with the expression lag of *Wnt3a*. This finding is consistent with the result from a gain of function experiment using *Xenopus* embryo, from which Brewster *et al.* (19) proposed that *Xenopus Zic2* is a prepattern gene required for the differentiation of dorsal neural tube including its derivative. As determined by the BrdUrd assay, the cell proliferation was not significantly decreased in the dorsal neural tube of the *Zic2* mutant (data not shown) whereas the reduction of cerebellar granule cell proliferation was indicated in the *Zic1* mutant (7). These findings suggest that *Zic2* is essential for the timely differentiation of dorsal neural plate.

In addition to the intrinsic mechanism, we should consider that an extrinsic mechanism underlies NTD because the im-

paired development of the adjacent mesodermal structure is related to its occurrence (20). In fact, *Zic2* is expressed strongly in the sclerotome (6) and the open vertebral arches are observed even in the thoracic region of *Zic2*$^{kd/kd}$ embryo, in which the neural tube itself apparently was closed (spina bifida occulta). The vertebral defect in *Zic2*$^{kd/kd}$ embryo could be caused by the defect intrinsic to the neural plate in *Zic2*$^{kd/kd}$ mice because Wnt protein secreted from the roof plate has an influence on the development of somite derivatives (21).

In conclusion, multiple lines of evidence are presented demonstrating that Zic2 is required for the normal development of neural tissue. However, it still remains to be answered how *Zic2* regulates the progression of neurulation, or how the neurulation delay leads to NTD such as spina bifida.

We thank Dr. M. Mizuguchi for critical reading of the manuscript; Drs. S. Brown, N. Suzuki, H. Yaginuma, and T. Shiga for helpful advice and valuable discussions; Drs. A. P. McMahon, S. Takada, and T. Saito for *in situ* probes; Mr. K. Auguste for helpful comments on the manuscript; and Ms. M. Yakuwa, Y. Nishi, and M. Nakashima for technical assistance. This work was supported by Special Coordination Funds for Promoting Science and Technology, CREST (Core Research for Evolutional Science and Technology) of Japan Science, Special Postdoctoral Researchers Program of RIKEN, Japan Society for Promotion of Science, and grants from the Japanese Ministry of Education, Science, and Culture.

1. Edmonds, L. D. & James, L. M. (1990) *Morbid. Mortal. Wkly. Rep*. **39,** 19–23.
2. Ming, J. E. & Muenke, M. (1998) *Clin. Genet.* **53,** 155–163.
3. Brown, S. A., Warburton, D., Brown, L. Y., Yu, C., Roeder, E. R., Stengel-Rutkowski, S., Hennekam, R. C. M. & Muenke, M. (1998) *Nat. Genet.* **20,** 180–183.
4. Benedyk, M. J., Mullen, J. R. & DiNardo, S. (1994) *Genes Dev.* **8,** 105–111.
5. Aruga, J., Nagai, T., Tokuyama, T., Hayashizaki, Y., Okazaki, Y., Chapman, V. M. & Mikoshiba, K. (1996) *J. Biol. Chem.* **271,** 1043–1047.
6. Nagai, T., Aruga, J., Takada, S., Gunther, T., Sporle, R., Schughart, K. & Mikoshiba, K. (1997) *Dev. Biol.* **182,** 299–313.
7. Aruga, J., Minowa, O., Yaginuma, H., Kuno, J., Nagai, T., Noda, T. & Mikoshiba, K. (1998) *J. Neurosci.* **18,** 284–293.
8. Suzuki, A., Nagai, T., Nishimatsu, S., Sugino, H., Eto, Y., Shibai, H., Murakami, K. & Ueno, N. (1994) *Biochem. J.* **298,** 275–280.
9. Saito, T., Lo, L., Anderson, D. J. & Mikoshiba, K. (1996) *Dev. Biol.* **180,** 143–155.
10. Hogan, B., Beddington, R., Constantini, F. & Lacy, E. (1994) *Manipulating the Mouse Embryo* (Cold Spring Harbor Lab. Press, Plainview, New York).
11. Green, M. R. (1989) *Curr. Opin. Cell Biol.* **1,** 519–525.
12. Takahashi, S., Onodera, K., Motohashi, H., Suwabe, N., Hayashi, N., Yanai, N., Nabeshima, Y. & Yamamoto, M. (1997) *J. Biol. Chem.* **272,** 12611–12615.
13. Stuart, E. T., Kioussim, C. & Gruss, P. (1994) *Annu. Rev. Genet.* **28,** 219–236.
14. Echelard, Y., Epstein, D. J., St-Jacques, B., Shen, L., Mohler, J., McMahon, J. A. & McMahon, A. P. (1993) *Cell* **75,** 1417–1430.
15. Takada, S, Stark, K. L., Shea, M. J., Vassileva, G., McMahon, J. A. & McMahon, A. P. (1994) *Genes Dev.* **8,** 174–189.
16. Brown, S., Russo, J., Chitayat, D. & Warburton, D. (1995) *Am. J. Hum. Genet.* **57,** 859–866.
17. Roessler, E., Belloni, E., Gaudenz, K., Jay, P., Berta, P., Scherer, S. W., Tsui, L. C. & Muenke, M. (1996) *Nat. Genet.* **14,** 357–360.
18. Chiang, C., Litingtung, Y., Lee, E., Young, K. E., Corden, J. L., Westphal, H. & Beachy, P. A. (1996) *Nature (London)* **383,** 407–413.
19. Brewster, R., Lee, J. & Ruiz i Altaba, A. (1998) *Nature (London)* **393,** 579–583.
20. van Straaten, H. W., Hekking, J. W., Consten, C. & Copp, A. J. (1993) *Development (Cambridge, U.K.)* **117,** 1163–1172.
21. Ikeya, M. & Takada, S. (1998) *Development (Cambridge, U.K.)* **125,** 4969–4976.